Computers in Biology and Medicine 197 (2025) 111073

Contents lists available at ScienceDirect

Computers in Biology and Medicine

journal homepage: www.elsevier.com/locate/compbiomed

Skeletal muscle death from the perspective of electrical impedance as evidenced by experiment and numerical modelling

Rok Šmerc, Damijan Miklavčič, Samo Mahnič-Kalamiza *

University of Ljubljana, Faculty of Electrical Engineering, Tržaška cesta 25, SI-1000, Ljubljana, Slovenia

ARTICLE INFO

Keywords:
Tissue electrical impedance
Ex vivo animal tissue
Numerical modelling
Skeletal muscle anisotropy
Electroporation

ABSTRACT

Understanding the biophysical changes in skeletal muscle tissue during the minutes to hours post-excision or following irreversible damage is critical for biomedical applications and food processing. Muscle tissue, composed of myofibrillar and sarcoplasmic proteins, water, lipids, and connective tissue, forms a complex network of interactions that persists as it degrades post-mortem. This study investigates skeletal muscle death through ex vivo experimental measurements on porcine muscle, supported by a novel numerical model that builds the muscle up from individual fibres. Skeletal muscle tissue was found to exhibit strong anisotropy in electrical conductivity due to its structure. It demonstrates much lower conductivity perpendicular to muscle fibres compared to parallel with them owing to its limited plasma membrane conductivity. We explore how post-mortem changes, including increased membrane permeability during membrane decomposition, and external interventions like electroporation, alter these anisotropic properties. Our findings have implications for biomedicine, specifically treatments targeting muscle tissue, such as pulsed field ablation for cardiac arrhythmias, and characterisation of in-vitro engineered muscle tissues. In food production, the study informs applications of pulsed electric fields to modify meat structure and texture. By integrating experimental and theoretical approaches, this work provides new insights into the electrochemical and structural dynamics of skeletal muscle during and after death.

1. Introduction

Biological tissues exhibit complex electrical properties that are determined by their composition, structure, and the distribution of ions and polar molecules within. These properties influence the behaviour of electric field and current flow in tissue and vary greatly between different tissues and tissue constituents [1–6]. For example, extracellular spaces typically exhibit higher conductivity due to the presence of free ions, whereas cell membranes, with their significantly lower electrical conductivity, act as insulating barriers that impede current flow [7,8]. In addition, tissue properties are also frequency-dependent, with different structures and processes characterising the electrical response of the tissue across different frequency ranges [4,6]. Knowledge of tissue properties is fundamental to understanding the behaviour of tissue in response to electrical stimuli, which is crucial both for clinical applications and for the development or optimisation of new biomedical technologies. These applications include electrical stimulation therapies [9–12], diagnostic imaging techniques [13,14] and electroporation-based treatments [15–17].

Electroporation is a biophysical phenomenon where short, high-voltage electrical pulses temporarily permeabilise cell membranes, allowing ions and molecules, such as drugs or nucleic acids, to enter/exit the cells. Depending on the pulse parameters, electroporation can be reversible, where cells recover after the membrane resealing, or irreversible, which leads to cell death [18–20]. Both reversible and irreversible electroporation are used in a wide variety of fields, from biomedicine and biotechnology to the food industry [16,17,21–25]. Reversible electroporation is commonly used for gene electrotransfer or drug delivery, with skeletal muscle being the predominant target [26–28]. In contrast, pulsed field ablation, a treatment modality that is based on irreversible electroporation, is advancing the treatment of cardiac arrhythmias, particularly atrial fibrillation, through pulmonary vein isolation [29–32]. The end goal of pulsed field ablation is to irreversibly damage the target tissue, resulting in cessation of conduction of electrical signals that cause arrhythmias. It is therefore of great interest and importance to the success of this treatment that we understand the mechanisms of muscle cell death, as well as how electroporation affects the target tissue properties such as electrical impedance, as this

* Corresponding author. University of Ljubljana, Faculty of Electrical Engineering, Laboratory of Biocybernetics, Tržaška cesta 25, SI-1000 Ljubljana, Slovenia.
E-mail address: samo.mahnic-kalamiza@fe.uni-lj.si (S. Mahnič-Kalamiza).

https://doi.org/10.1016/j.compbiomed.2025.111073
Received 6 May 2025; Received in revised form 5 September 2025; Accepted 8 September 2025
Available online 13 September 2025

impedance will govern current flow (and electric field distribution) through the target tissue post-treatment.

In the food processing industry, the phenomenon of electroporation falls under the umbrella of a wider, more encompassing term *pulsed electric fields* treatment, which is more related to the method of altering the tissue rather than the phenomenon of increased membrane permeability itself, since it is with intense electrical pulses used to pre-treat various food matrices that the intended disruption of cell membranes, microorganisms, or enzymes is achieved resulting in a desired effect. The treatment, well established for processing of plant materials, is also being examined for its potential in the meat industry for e.g. tenderisation, as it can improve meat tenderness by disrupting muscle fibres and enzymatic activity [33], enhancing drying and curing [34], and for improving quality by reducing cooking time and improving texture during sous-vide processing [35]. However, there are many open questions as to the exact mechanisms by which pulsed electric fields affect muscle tissue. This void is exacerbated by large biological diversity in the raw material (animal species, tissue type and origin, etc.) and a plethora of possible combinations of treatment parameters, both electrical and other physical conditions (e.g. temperature, time post-mortem, etc.) [33,36]. This variability and wide-open parameter space produce a need to not only characterise the treated material from the electrical perspective to ensure success and homogeneity of the treatment by pulsed electric fields, but also to provide means of detecting and quantifying the effects of the treatment in the target tissue.

Regardless of whether we are interested in the response of muscle tissue to electric fields for purposes of biomedical or food processing applications, it is important to note that both skeletal and cardiac muscles exhibit directional differences in their electrical properties, a property known as anisotropy [37–39]. The anisotropy in skeletal and cardiac muscles arises from the alignment of the muscle fibres, which are embedded in a complex network of connective tissue layers [40,41]. These layers, together with the insulating sarcolemma, form a unique arrangement that restricts the movement of ions in certain directions, resulting in different electrical properties that vary depending on fibre orientation, especially at low frequencies [42]. Electrical conductivity is usually higher in the direction of the muscle fibres than across them [4,6]. Interestingly, even tissues that are not intrinsically anisotropic, such as liver tissue, can develop anisotropic properties after electroporation [43]. The characterisation of anisotropic behaviour is important for understanding how electrical stimuli influence the tissue response.

Electrical impedance spectroscopy (EIS) is a powerful technique for characterising the electrical properties of biological tissue over a wide frequency range. By applying a small alternating current (AC) and measuring the resulting voltage, EIS provides information on both the resistive and capacitive properties of tissues [44–46]. Through analysis of the impedance spectrum, important insights into how tissues respond to external electrical stimuli are provided, aiding in the evaluation of treatment outcomes. Furthermore, EIS can be effectively used to characterise anisotropic tissue properties, distinguishing electrical behaviour along and across the fibre axis [3,4,47]. Its non-invasive and real-time capabilities make it an indispensable tool in both clinical and research settings, enabling the exploration of the intricate relationship between tissue structure, composition, and electrical properties. In addition, EIS enables the evaluation of dynamic changes in tissue properties, such as those induced by electroporation [48–51] or occurring post-mortem [52–54]. There is even an established methodology of assessing the integrity of the cell membranes using EIS – the P_y parameter of meat quality, which relates the degree of meat degradation post-mortem to the meat quality properties such as drip/cooking/frying loss, pH, colour, etc. [55].

In addition to EIS, there are alternative methods for assessing the electrical properties of tissue, such as analysing voltage and current waveforms recorded during the application of electrical pulses. Monitoring these electrical signals in real time provides valuable insight into changes in membrane properties during electroporation [56,57]. Current dynamics during the application of high-voltage pulses have been shown to be indicative of electroporation processes, further highlighting the potential of this approach to characterise tissue responses. While less frequently employed, these analyses complement EIS by providing additional information on tissue behaviour during and after electroporation [58,59].

The aim of the present study was threefold: first, to assess whether skeletal muscle anisotropy can be shown by impedance spectroscopy measurements in ex vivo tissue post-mortem, second, to validate the experimental results by numerical modelling with emphasis on the permeability of the plasma membrane, and third, to show whether loss of integrity of the skeletal muscle cell plasma membrane resulting from phospholipase activity and other degradation processes can be likened, in effect, to increasing cell membrane permeability by electroporation. We sought to assess the feasibility of characterising the anisotropic properties of the tissue ex vivo, several hours post-mortem, when cellular and structural changes may alter the electrical behaviour of the tissue. In addition, we analysed the current dynamics during the application of high-voltage pulses to complement the impedance data, allowing for a more comprehensive analysis of tissue responses. The primary key objective was to demonstrate that muscle tissue can serve as a reliable model for in vivo tissue even a few hours post-mortem. This offers an alternative to experiments with living animals and in turn reduces the ethical burden of animal testing in medical research. The secondary key objective was to demonstrate that i) electroporation as a mechanism of increasing cell membrane permeability (and current conductivity) and ii) breaking down of the structural components of the membrane through phospholipase activity leading to membrane thinning and increased permeability [60], both impact the muscle anisotropy in the same sense, thus demonstrating that the muscle cell plasma membrane is indeed the structure responsible for anisotropy of living muscle tissue electrical impedance.

2. Materials and methods

2.1. Experimental setup

The experimental setup for the impedance spectroscopy experiments comprised an LCR metre, a pulse generator, an oscilloscope, a treatment chamber, and a PC running LabVIEW for data acquisition and control. The LCR metre (model E4980A, Keysight Technologies, Santa Rosa, CA, USA) was used to perform impedance measurements, while the laboratory prototype pulse generator (HV-LV) [56] was used to deliver high-voltage electroporation pulses. The oscilloscope (model HDO6104A-MS, LeCroy, Chestnut Ridge, NY, USA), equipped with voltage (model HVD3206A, LeCroy, Chestnut Ridge, NY, USA) and current (model CP031A, LeCroy, Chestnut Ridge, NY, USA) probes, was used to monitor and verify the electrical pulses generated by the pulse generator. A custom-built acrylic treatment chamber with a diameter of 26 mm was used to house the tissue samples during the experiments. The chamber was equipped with two pairs of custom-made stainless-steel electrodes spaced 6 mm apart, which were used both for delivering the high-voltage electroporation pulses and for impedance measurements. These electrodes were configured for 4-electrode impedance measurements to ensure accurate and reliable data acquisition. Stainless-steel was selected for electrode material as it provides sufficient stability and durability for high-voltage pulsing and is safe to use, since, in the 4-electrode configuration employed, the influence of electrode polarisation is minimised, making the use of non-polarisable materials such as platinum unnecessary. A switch box was integrated into the setup to allow seamless switching between the LCR metre and pulse generator connections to the electrodes. The PC running LabVIEW (version LabVIEW 2020, National Instruments, Austin, TX, USA) controlled the data acquisition and enabled automated measurement procedures and real-time data monitoring. A photograph of the experimental setup with the individual components is shown in Fig. 1.

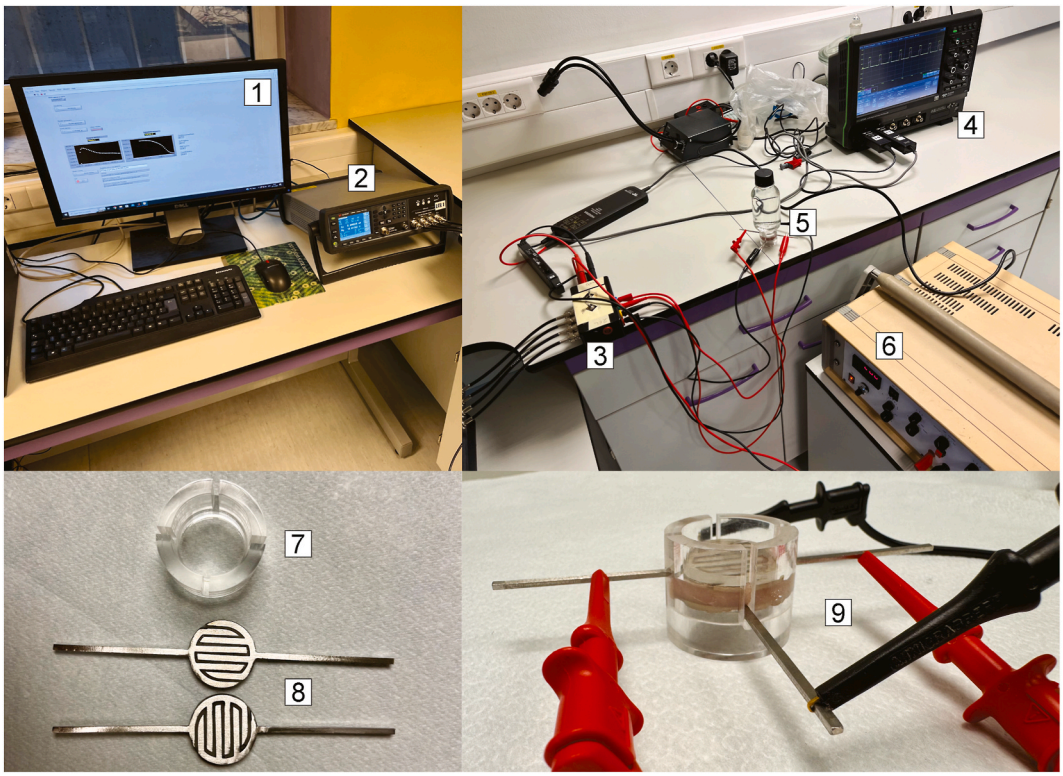

Fig. 1. Experimental setup for impedance spectroscopy experiments. The setup consists of (1) a PC running LabVIEW for data acquisition and control, (2) an LCR metre for performing impedance measurements, (3) a switch box that allows switching between the connections of the LCR metre and the pulse generator to the electrodes, (4) an oscilloscope with voltage and current probes for signal monitoring, (5) a treatment chamber with two pairs of electrodes and a tissue sample between the pairs, (6) a laboratory prototype pulse generator, (7) a treatment chamber made of acrylic glass, (8) two pairs of stainless steel electrodes used for 4-electrode impedance measurements within the treatment chamber, and (9) a tissue sample.

2.2. Preparation of muscle tissue samples

The muscle tissue used in the experiments was obtained from the trapezius muscle of a pig (*Sus scrofa domesticus*), which was harvested within a half-hour after death. The tissue was sourced from a slaughterhouse that operates according to Slovenian law. To ensure consistency of the impedance measurements, a muscle with a uniform orientation of the fibres was selected. This allowed a reliable comparison of impedance measurements in both parallel and perpendicular orientations relative to the fibres. After harvesting, the tissue was cooled to 4 °C to preserve its structure and properties. As the measurements could not be performed immediately due to the time required for tissue harvesting, transport to the laboratory, and sample preparation, the first measurements were performed approximately 3 h post-mortem. Before each series of experiments, which were conducted at three different time points (3 h, 24 h, and 72 h post-mortem), the tissue samples were allowed to warm up to room temperature. A sharp cork borer was used to manually cut discs of 26 mm diameter from the tissue sample. The thickness of the discs was 6 mm. Two types of samples were prepared: one set was cut so that the impedance measurements could be performed along the muscle fibres (parallel orientation), and the other set was prepared so that the measurements could be performed across the muscle fibres (perpendicular orientation).

2.3. Impedance spectroscopy and pulse dynamics analysis

Impedance spectroscopy measurements were conducted on untreated muscle tissue at three different post-mortem time points: 3 h, 24 h, and 72 h. These baseline measurements were performed to characterise the electrical properties of the tissue in both parallel and perpendicular orientations relative to the muscle fibres. At each time point, six replicates of the experiment were performed ($N = 6$) to ensure statistical reliability. Absolute impedance and phase angle were measured in the frequency range from 20 Hz to 2 MHz. The frequency sweep comprised 40 logarithmically spaced points, corresponding to 8 points per decade, to ensure a uniform resolution over the entire frequency range. A sinusoidal voltage of 100 mV peak was applied to one pair of electrodes. This pair served as the current source and sink, while the other pair was used to measure the voltage drop, as customarily configured in 4-electrode impedance analysis. The selected frequency range allowed for characterisation of the tissue's electrical properties over a broad range and reflected the maximum measurement capability of the LCR meter used (Keysight E4980A).

Following the baseline impedance measurements, electroporation pulses were applied to the tissue samples at the 3-h and 24-h post-mortem time points, but not at 72-h post-mortem (see Discussion for an explanation). The impedance measurements were recorded again within 2 s after pulse delivery (allowing for the time to switch the electrodes from the generator to the LCR meter). Electroporation was performed using eight rectangular pulses, each with a duration of 100 μs, an amplitude of either 200 V or 400 V, and a pulse repetition rate of 1 s^{-1}. Pulse amplitudes were selected to induce different degrees of electroporation, with 200 V producing moderate effects and 400 V resulting in more extensive membrane permeabilisation. The ratio of the impedance magnitude after electroporation ($|Z_{post}|$) to the impedance magnitude before electroporation ($|Z_{pre}|$) was calculated for each sample to quantify the effect of electroporation on the impedance of the tissue. Results are expressed as mean ± standard deviation.

In addition, the pulse dynamics during the electroporation pulses were analysed. The normalised electrical current difference (ΔI_{norm}) was calculated to quantify the change in current during the first delivered pulse, similar to the approach used previously [61]. We defined ΔI_{norm}

as the difference between the final current (I_f) at $t = 95$ μs (determined as the average value of the current between 94.5 and 95.5 μs to eliminate measurement noise) and the initial current (I_i) at $t = 5$ μs (average value of the current between 4.5 and 5.5 μs), divided by the initial current (I_i), as shown in the following equation:

$$\Delta I_{\text{norm}} = \frac{I_f - I_i}{I_i}. \tag{1}$$

We chose the current as recorded at 5 μs as the initial current to allow for all the transients in the current waveform (e.g. capacitive spike at the start of the pulse) to completely fade consistently (for all pulses). The sample that represents the final current value (at 95 μs) was chosen to consistently capture the highest current value before the pulse starts to decrease in amplitude.

To assess the statistical significance of the results, Student's t-test was used to compare the current differences at different orientations and time points. All statistical analysis and data processing were performed using Python.

2.4. Numerical modelling

The simulations were conducted using COMSOL Multiphysics software (version 6.3, COMSOL AB, Stockholm, Sweden), employing the finite element method (FEM). To optimise computational efficiency, a simplified three-dimensional geometry was designed to approximate the experimental muscle tissue sample. The numerical model is based on the quasi-static approximation and solves the Laplace equation

$$\nabla\cdot((\sigma + j\omega\varepsilon_0\varepsilon)\nabla\varphi) = 0 \tag{2}$$

for the electric potential φ, with σ representing the conductivity in the intracellular, extracellular, and membrane regions, $j = \sqrt{-1}$, ω is the angular frequency, ε_0 is the permittivity of vacuum, and ε is the relative permittivity of the intracellular, extracellular, and membrane regions. The tissue was modelled as a cubic domain with dimensions of 1 mm per side, while the muscle fibres were represented as cylindrical structures extending over the entire domain, each with a diameter of 60 μm (see Fig. 2a). The volume fraction of the muscle fibres was set at 78 %, which corresponds to typical values reported in the literature for skeletal muscle tissue [62]. In our previous work [63], we showed that variations in volume fraction had no significant effect on the anisotropy rate, supporting the use of a fixed value in the model. Since the cell plasma membranes are several orders of magnitude thinner than the other modelled dimensions, they were not explicitly included in the geometry. Instead, their electrical effect was incorporated through a boundary condition that represents the membrane as a thin resistive–capacitive layer. This condition relates the transmembrane current density to the local transmembrane voltage and accounts for both membrane conductivity and permittivity. The membrane's thickness was used together with its electrical properties to define the specific impedance of the boundary [64,65]. Mathematically, the boundary condition is expressed as

$$n\cdot J = \frac{1}{d_m}(\sigma_m + j\omega\varepsilon_0\varepsilon_m)(V_i - V_e), \tag{3}$$

where n is the normal vector, J is the current density, d_m is the membrane thickness, σ_m and ε_m are the membrane conductivity and relative permittivity, respectively, and V_i and V_e are the electric potentials on the intracellular and extracellular sides of the membrane, respectively.

The electrodes were positioned in two different orientations with respect to the muscle fibre alignment (see Fig. 2b). In the parallel orientation, the electrodes were placed so that the impedance was measured along the direction of the muscle fibres, whereas in the perpendicular orientation, the impedance was measured perpendicular to the fibre orientation. The simulations were performed in the frequency domain to compute the steady-state electric potential

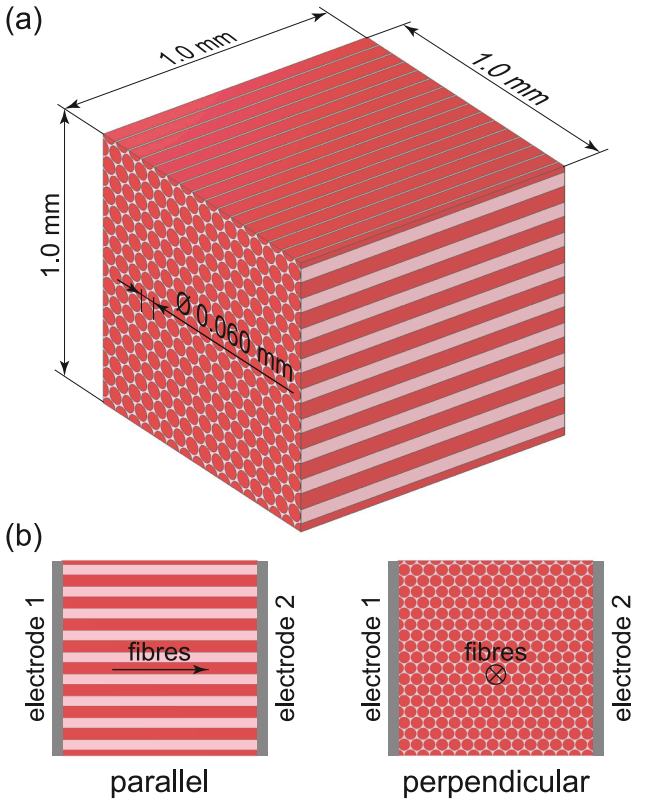

Fig. 2. (a) Geometry and dimensions of the muscle tissue model in COMSOL Multiphysics. (b) The two orientations of the electrodes relative to the orientation of the muscle fibres: in the parallel orientation, the electrodes are positioned so that the impedance is measured in the direction parallel to the muscle fibres; in the perpendicular orientation, the impedance is measured perpendicular to the fibre orientation.

distribution across the model at each frequency. This allowed us to determine the frequency-dependent impedance of the tissue, enabling direct comparison with the experimental measurements in the 20 Hz to 2 MHz range. The finite element mesh comprised approximately 1.9 million elements, with second-order (quadratic) Lagrange elements used for potential discretisation. A mesh convergence check was performed to ensure numerical stability, confirming that the computed impedance values remained consistent with finer mesh resolutions.

The main objective of the simulations was to calculate the impedance in both parallel and perpendicular orientations at 3 h and 24 h post-mortem experimental conditions, when the anisotropy is still observed. A parametric study was conducted to evaluate the effect of varying plasma membrane conductivities on the impedance predictions of the model. Membrane conductivities were adjusted to simulate changes in tissue properties over time. The results for the different membrane conductivities were then compared with the experimental measurements at 3 h and 24 h post-mortem. The best-fit conductivity values for the membranes at each time point were determined using the least mean squares method. The impedance values obtained from the model were adjusted to take into account the differences in dimensions between the model and the experimental setup. The calculated impedance was adjusted using the following equation:

$$|Z_{\text{adjusted}}| = |Z_{model}|\cdot\frac{k_1}{k_2}, \tag{4}$$

where $|Z_{\text{adjusted}}|$ is the adjusted impedance, $|Z_{\text{model}}|$ is the impedance calculated by the model, k_1 is a scaling factor for electrode spacing, and k_2 is a scaling factor that accounts for electrode surface area. In the experimental setup, the distance between the electrodes was 6 mm,

whereas in the numerical model it was 1 mm, yielding $k_1 = 6$. The area of each electrode in the experimental setup was 179.71 mm^2, compared to 1 mm^2 in the model, yielding $k_2 = 179.71$. Although only the ratio k_1/k_2 affects the impedance scaling, we define the two factors separately to preserve a clear connection to the distinct geometric differences between the model and experimental setups. This adjustment ensures that the model impedance results are directly comparable with experimental measurements.

The parameters used in the model and their corresponding values are listed in Table 1. The relative permittivity of the membranes was increased compared to the typically used values for the relative permittivity of the membranes in order to take into account the connective tissue layers surrounding the muscle fibres, which were not explicitly included in the geometry of the model. Membrane conductivity was not modelled as a function of transmembrane voltage. Instead, it was treated as a constant parameter within each simulation, and varied only across different simulations to reflect changes in membrane integrity due to post-mortem degradation. This adjustment was important to better represent the electrical properties of the tissue and to ensure that the model reflected the experimentally observed impedance changes. It is important to note that while COMSOL Multiphysics was used for simulations, the underlying model is fundamentally based on well-known principles of bioelectricity and can be reproduced using any numerical method that solves the quasi-static Laplace equation with the same boundary conditions and parameter settings applied. In summary, the novelty of our modelling approach lies in representing muscle tissue at the level of individual fibres. This structural model allows for anisotropy to emerge naturally from the geometry and electrical properties of the fibres, rather than relying on homogenised bulk tissue properties, providing direct insight into how changes in membrane conductivity influence macroscopic impedance behaviour. The post-processing of the simulation results was performed using Python.

3. Results and discussion

3.1. Impedance of untreated skeletal muscle

The frequency-dependent impedance of untreated skeletal muscle was measured at three post-mortem time points to assess the changes in the electrical properties of the tissue over time, focusing on the anisotropy between the two orientations with respect to the muscle fibres: the parallel (i.e., the impedance was measured in the direction parallel to the muscle fibres) and the perpendicular (i.e., the impedance was measured in the direction perpendicular to the muscle fibres).

At 3 h post-mortem, significant differences in skeletal muscle impedance can be observed between the parallel and perpendicular orientations (Fig. 3a), with the perpendicular orientation exhibiting more than 10 times higher impedance at lower frequencies. This pronounced anisotropy is due to the fibrous structure of skeletal muscle and the preservation of cell plasma membranes shortly (at minimum 3 h) after death, resulting in significantly different impedance characteristics between the two orientations. The resistance curves (Fig. 3b) closely resemble the impedance curves, suggesting that the measured impedance is predominantly resistive in nature. In the parallel orientation, the resistance values are substantially lower over the entire frequency range than in the perpendicular orientation. At very low frequencies (below 100 Hz), the resistance in the parallel orientation falls below zero, which is not physically meaningful and likely reflects measurement artefacts due to very low impedance values, poor signal-to-noise ratio, and reactive dominance at these frequencies. These deviations are likely caused by the limitations of the measurement equipment, even when a four-electrode configuration is used. The reactance (Fig. 3c) shows a markedly different behaviour between the two orientations. In the parallel orientation, the reactance remains close to zero across all frequencies, indicating minimal capacitive effects. In contrast, the perpendicular orientation shows negative reactance values, which are characteristic of capacitive behaviour. The largest magnitude of reactance (i.e., the most negative value) occurs at around 5 kHz. This behaviour reflects the capacitive charging and discharging of the intact cell membranes, which dominate the current flow at intermediate frequencies. At low frequencies, the membranes act as insulators, blocking current flow. As the frequency increases, the capacitive properties of the membranes allow displacement currents to pass, leading to a minimum of reactance. At high frequencies, the membranes become effectively transparent to the current and the reactance returns toward zero. In the parallel direction, where the current flows along the fibres, mostly bypassing the membranes, this capacitive behaviour does not occur.

Table 1
Parameters and their corresponding values used in the numerical model [66–69].

Parameter	Value	Description
f	0.78	Volume fraction of fibres
σ_i	0.80 S/m	Intracellular conductivity
σ_e	1.80 S/m	Extracellular conductivity
σ_m	varied	Membrane conductivity
ε_i	70	Intracellular relative permittivity
ε_e	80	Extracellular relative permittivity
ε_m	30	Membrane relative permittivity
d_m	4 nm	Membrane thickness
k_1	6	Adjustment factor
k_2	179.71	Adjustment factor

By 24 h post-mortem, the anisotropy remains, but the difference between the two orientations decreases, with the impedance in the perpendicular orientation being only about three times higher than in the parallel orientation (Fig. 3d). This reduction indicates the onset of cell degradation, including membrane disintegration, although the fibrous structure of the muscle still contributes to some anisotropy. The resistance curves (Fig. 3e) again closely follow the impedance curves, which confirms that the measured impedance remains primarily resistive. The reactance (Fig. 3f) in the parallel direction remains minimal, while the perpendicular orientation continues to show a negative reactance profile, indicating residual capacitive behaviour. Compared to the 3-h time point, the amplitude of this capacitive dip is reduced, and the frequency of the peak shift moves to around 20 kHz, consistent with progressive degradation of the membranes.

At 72 h post-mortem, there are no obvious differences in impedance (Fig. 3g), resistance (Fig. 3h), or reactance (Fig. 3i) between the two orientations. The impedance is equal in both directions and lower than at earlier time points, reflecting the loss of the muscle's structural integrity. These results highlight the progressive degradation of skeletal muscle tissue over time and the corresponding changes in electrical impedance, with the anisotropic behaviour in the early post-mortem stages attributed to the preservation of muscle structure and membranes, and the reduction in anisotropy corresponding to tissue breakdown.

Interestingly, in our previous study [70] where we looked at muscle anisotropy ex vivo using CDI (an MRI-based method of mapping current pathways in tissue), we have shown that 48 h post-mortem the electric current distribution still exhibits some anisotropy. Those CDI measurements have shown that current flows differently depending on whether it is injected into tissue perpendicular or parallel to the muscle fibres (two needle electrodes were used, rather than plate electrodes). This would seem to indicate that there is still some anisotropy present 48 h post-mortem, however, as we have shown with impedance measurements, all anisotropy is completely undetectable a day later, 72 h post-mortem.

The observed anisotropy in impedance measurements at 3 h post-mortem is consistent with findings reported in the literature, which collect data from various ex vivo skeletal muscle studies, some of which were conducted immediately after incision [3,4,6]. Although different methods were used in these studies, the anisotropic behaviour observed

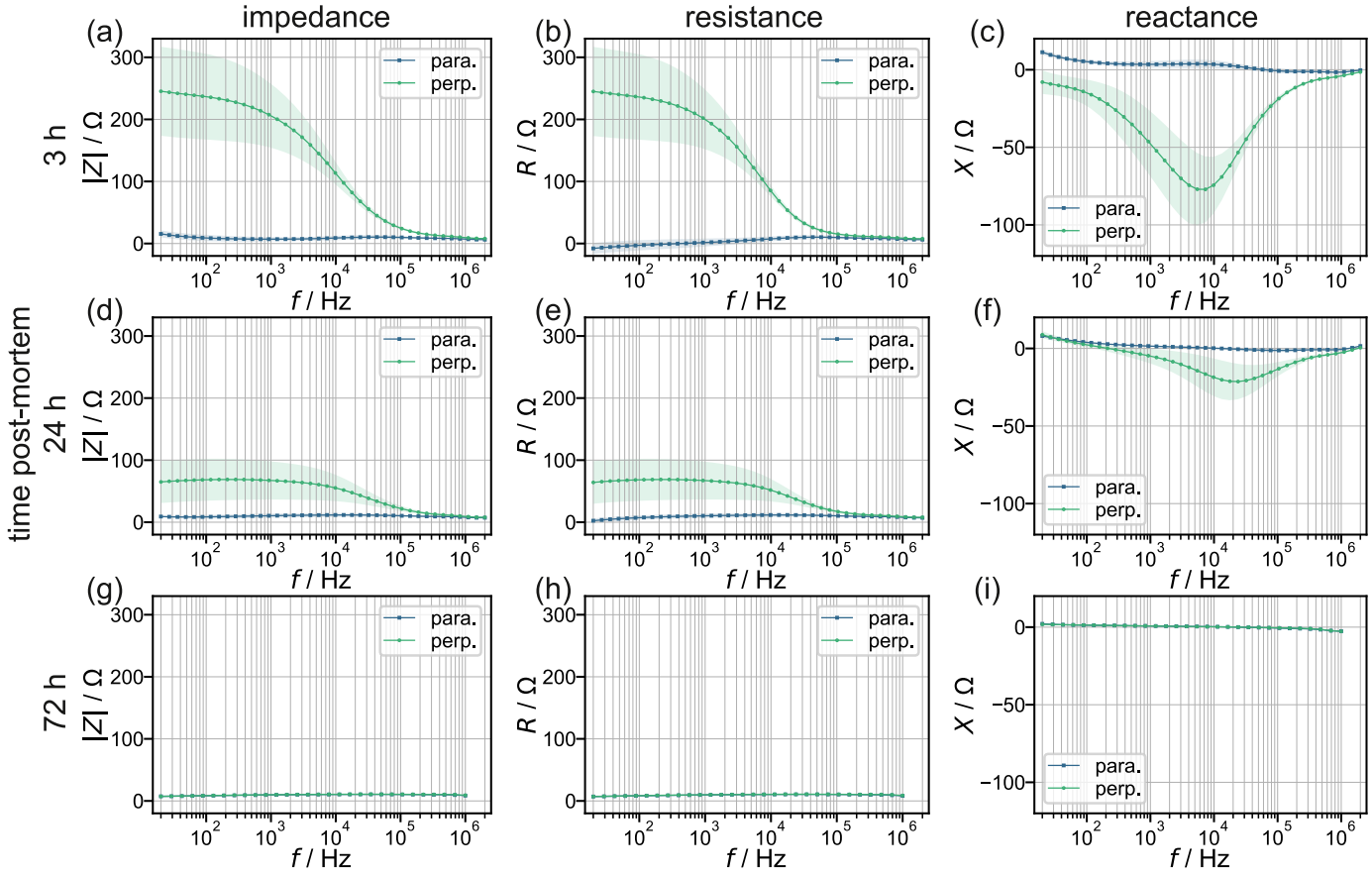

Fig. 3. Frequency-dependent absolute impedance (a, d, g), resistance (b, e, h), and reactance (c, f, i) of untreated skeletal muscle in the parallel (i.e., the impedance was measured in the direction parallel to the muscle fibres) and the perpendicular (i.e., the impedance was measured in the direction perpendicular to the muscle fibres) orientations at (a–c) 3 h post-mortem, (d–f) 24 h post-mortem, and (g–i) 72 h post-mortem. The results are given as mean values ± standard deviations (shaded areas), with $N = 12$.

in this work is consistent with the literature, supporting the feasibility of using post-mortem muscle tissue as a reliable model for in vivo tissue. However, it is important to emphasise that impedance measurements are influenced not only by the intrinsic electrical properties of the tissue, but also by the geometry of the measurement system, including the shape, size, and spacing of the electrodes. Detailed methods for determining the intrinsic electrical properties of anisotropic tissue in situ, independently of geometry, have been proposed in the literature [71, 72]. These approaches are usually based on specific electrode geometries and analytical approaches designed to extract directional conductivities and permittivities. However, such methods were beyond the scope of our current study, which instead focused on tracking how the anisotropy of impedance evolves over time post-mortem within a consistent and well-defined experimental geometry.

3.2. Electroporation-induced changes in skeletal muscle impedance

The effect of electroporation on the electrical properties of skeletal muscle tissue was investigated by measuring the frequency-dependent impedance before ($|Z_{pre}|$) and after ($|Z_{post}|$) electroporation, with the impedance ratio ($|Z_{post}|/|Z_{pre}|$) serving as a measure of the electroporation-induced changes. Electroporation was performed using 8 rectangular pulses, each with a duration of 100 µs, with amplitudes of 200 V or 400 V, and at a pulse repetition rate of 1 s^{-1}. The results for both 3 h and 24 h post-mortem are shown in Fig. 4. We chose not to perform electroporation experiments 72 h post-mortem since, as is evident in Fig. 3g, there is no observable anisotropy even in intact tissue.

At 3 h post-mortem, the impedance ratio showed marked changes in the response to electroporation in both the parallel and perpendicular orientations. Following the application of 200 V pulses, the impedance decreased by about 10 % in the parallel orientation (Fig. 4a) and by about 15 % in the perpendicular orientation (Fig. 4b), as shown in Fig. 4c. This modest reduction indicates that pulses with an amplitude of 200 V are not sufficient to induce major changes in the electrical properties of muscle tissue. However, increasing the amplitude to 400 V resulted in a much stronger effect. In the parallel orientation, the impedance decreased by up to 20 % (Fig. 4d), while in the perpendicular orientation the decrease was about 60 % (Fig. 4e), as can be seen from the impedance ratio (Fig. 4f). These larger decreases at higher amplitudes indicate that the 400 V pulses caused significant electroporation, disrupting plasma membranes and significantly altering the electrical properties of the tissue.

At 24 h post-mortem, the impedance changes were less pronounced, likely due to tissue degradation. In the parallel orientation, 200 V pulses caused minimal impedance changes, with no significant reduction observed (Fig. 4g). However, in the perpendicular orientation, a reduction of a similar magnitude to that observed in the samples collected 3 h post-mortem was still observed (Fig. 4h), as shown in Fig. 4i. When the amplitude was increased to 400 V, the changes in the parallel orientation were again minimal (Fig. 4j). In contrast, the impedance in the perpendicular orientation decreased by approximately 30 % (Fig. 4k), as shown in Fig. 4l, demonstrating a weaker but still observable effect compared to the 3 h post-mortem. This reduction in the magnitude of the impedance change 24 h post-mortem suggests that as the tissue degrades, its susceptibility to electroporation decreases, likely due to the degradation of cellular structures and plasma membranes.

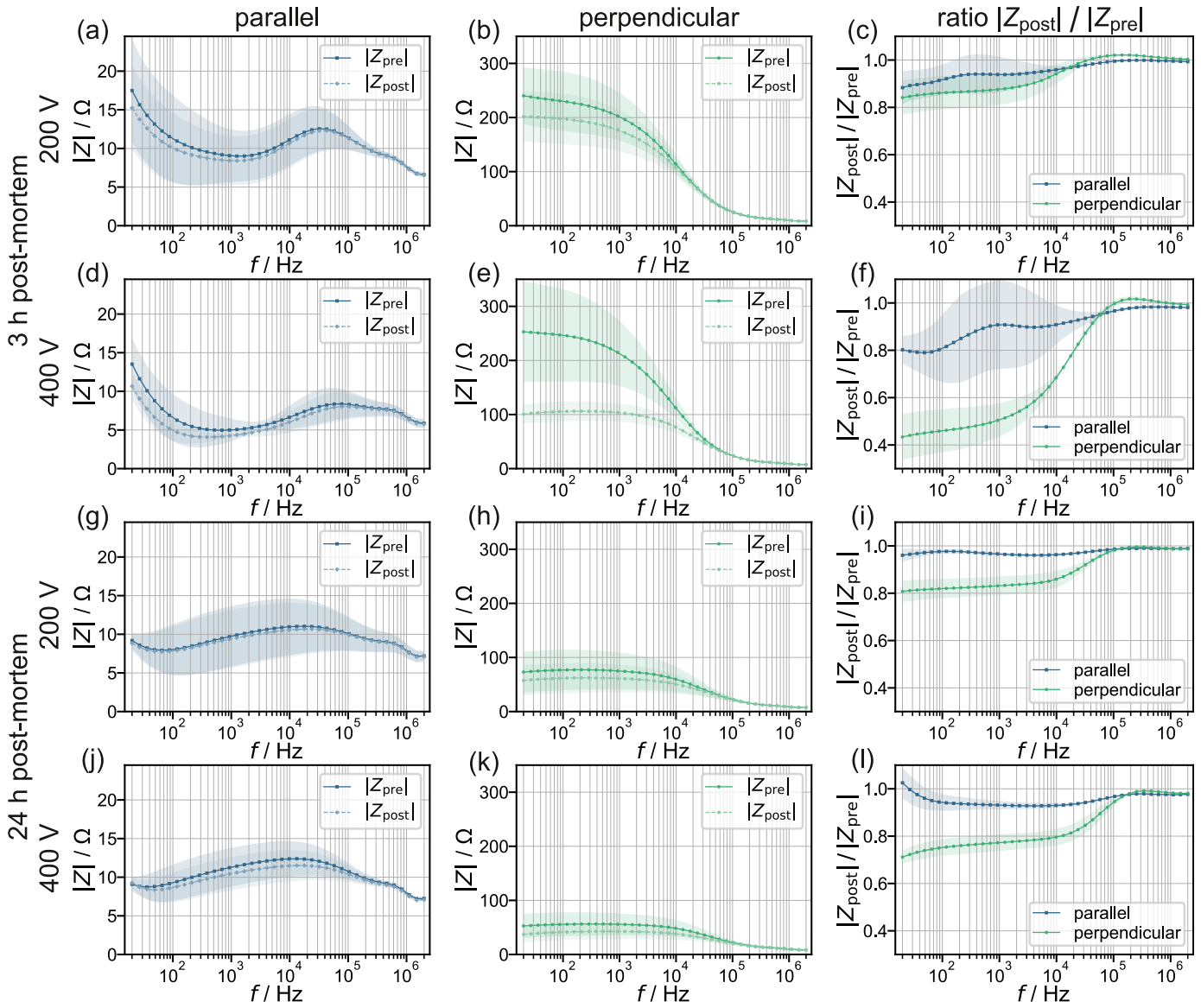

Fig. 4. Frequency-dependent absolute impedance of untreated skeletal muscle (i.e., before electroporation; $|Z_{pre}|$), treated skeletal muscle (i.e., within 2 s after electroporation; $|Z_{post}|$), and their ratio ($|Z_{post}|/|Z_{pre}|$), measured in the parallel (i.e., the impedance was measured in the direction parallel to the muscle fibres) and the perpendicular (i.e., the impedance was measured in the direction perpendicular to the muscle fibres) orientations. Electroporation was performed using 8 rectangular pulses, each with a duration of 100 μs, an amplitude of either 200 V or 400 V, and a pulse repetition rate of 1 s^{-1}. The results for 3 h post-mortem are shown in (a–f), and for 24 h post-mortem in (g–l). The amplitude of the applied pulses was 200 V in (a–c, g–i) and 400 V in (d–f, j–l). The absolute impedance of untreated and treated skeletal muscle, measured in the parallel orientation, is shown in (a, d, g, j), and in the perpendicular orientation in (b, e, h, k). The impedance ratio ($|Z_{post}|/|Z_{pre}|$) is shown in (c, f, i, l). The results are given as means ± standard deviations (shaded areas), with $N = 6$. Note the different ordinate scales for absolute impedance measured in the parallel (a, d, g, j) and perpendicular (b, e, h, k) orientations.

Although the observed changes in impedance after electroporation (Fig. 4a, b, 4d, 4e, 4g, 4h, 4j, 4k) appear small and statistically insignificant in most cases, except for the perpendicular orientation with 400 V pulses (Fig. 4e), it is important to note that electroporation consistently decreased tissue impedance in each pair of before-after measurements. The relatively large standard deviations observed are attributable to variability between different tissue samples.

The observed results indicate that the efficacy of electroporation on skeletal muscle impedance is time-dependent, with a stronger effect at earlier post-mortem stages when tissue integrity is better preserved. At 3 h post-mortem, electroporation with 400 V pulses resulted in a significant decrease in impedance, particularly in the perpendicular orientation. This significant decrease in the perpendicular orientation can be attributed to the orientation of the muscle fibres and cell plasma membranes relative to the applied electric field. In the perpendicular orientation, the membranes lie in the path of the electric field and are directly electroporated, which leads to significant impedance changes. In contrast, in the parallel orientation, the membranes are aligned along the field and do not present a significant barrier, resulting in smaller impedance changes. At 24 h post-mortem, the effect of electroporation was significantly attenuated, reflecting the progressive loss of tissue structure and functionality as well as reduced membrane integrity.

The observed anisotropic effects on impedance changes after electroporation provide a mechanistic explanation for the differences in lesion shapes observed in skeletal [63] and cardiac [73] muscles when electric fields are applied in different orientations. Electroporation in the perpendicular orientation resulted in significantly greater impedance decrease, indicating more extensive cell plasma membrane disruption compared to the parallel orientation. This is consistent with the structural arrangement of the muscle fibres, where the membranes are more

exposed to the electric field in the perpendicular orientation, leading to greater conductivity changes. In the parallel orientation, the field is aligned with the fibres, bypassing membranes and causing less disruption. These differences have a direct influence on permeabilisation (e.g. in DNA delivery by electroporation) and on lesion formation in electroporation-based ablation procedures. Lesions in the parallel orientation are narrower and less extensive, while lesions in the perpendicular orientation are larger and more widespread.

Existing models often assume the same factor of conductivity increase for both parallel and perpendicular orientations and maintain a constant anisotropy ratio (the ratio of parallel to perpendicular conductivity) before and after electroporation [32,73–76]. Even though these models are focused on cardiac muscle, we can reasonably assume that our findings from skeletal muscle are at least partially transferable to cardiac muscle, as both tissues exhibit anisotropic properties due to their fibrous structure. We have observed that the impedance is much less affected by electroporation in the parallel orientation, suggesting that the factor of conductivity increase should be much lower in the parallel orientation than in the perpendicular orientation. This also means that the anisotropy ratio after electroporation should not be the same as before electroporation. Incorporating these findings into numerical models could increase their accuracy and enable better predictions about the distribution of the electric field and the formation of lesions.

3.3. Electric current dynamics during electroporation

The dynamics of the electric current during electroporation were evaluated by analysing the normalised electric current difference (ΔI_{norm}), which we defined as the difference between the final (I_f; at t = 95 μs) and initial (I_i; at t = 5 μs) current values of the first pulse delivered, normalised to the initial current value (I_i; see Fig. 5a). This parameter reflects the changes in electrical conductivity induced directly by electroporation. The results for the parallel and perpendicular orientations at 3 h and 24 h post-mortem are shown in Fig. 5b and c, respectively. The alternative comparison, focusing on comparing 3 h post-mortem versus 24 h post-mortem, is shown for 200 V and 400 V pulses in Fig. 5d and e, respectively.

At 3 h post-mortem (Fig. 5b), the normalised current difference showed significant differences between the parallel and perpendicular orientations, with the perpendicular orientation consistently exhibiting higher values. For 200 V pulses, the median normalised current difference in the parallel orientation was 0.12, while it was 0.29 in the perpendicular orientation ($p = 1.73 \times 10^{-5}$). A similar trend was observed for 400 V pulses, where the median of the normalised current difference was 0.04 in the parallel orientation and increased to 0.11 in the perpendicular orientation ($p = 1.58 \times 10^{-4}$).

At 24 h post-mortem (Fig. 5c), the values of the normalised current difference were significantly lower, indicating the influence of tissue degradation on the electroporation dynamics. For 200 V pulses, the median normalised current difference in the parallel orientation had decreased to 0.04, with respect to 0.12 in the perpendicular orientation. For 400 V pulses, the medians were 0.03 in the parallel orientation and 0.06 in the perpendicular orientation. Statistical analysis confirmed significant differences between the two orientations for both 200 V ($p = 6.68 \times 10^{-4}$) and 400 V ($p = 1.66 \times 10^{-4}$).

When comparing the normalised current difference between 3 h and 24 h post-mortem (Fig. 5d and e), significant differences were found in most cases. For 200 V pulses (Fig. 5d), significant differences were observed in both orientations (parallel: $p = 6.12 \times 10^{-3}$; perpendicular: $p = 8.34 \times 10^{-6}$). For 400 V pulses (Fig. 5e), however, there was a significant difference in the perpendicular orientation ($p = 4.13 \times 10^{-4}$), while this was not the case for the parallel orientation ($p = 8.37 \times 10^{-2}$). These results suggest that the progressive degradation of cell plasma membranes over time reduces the ability of the tissue to undergo electroporation.

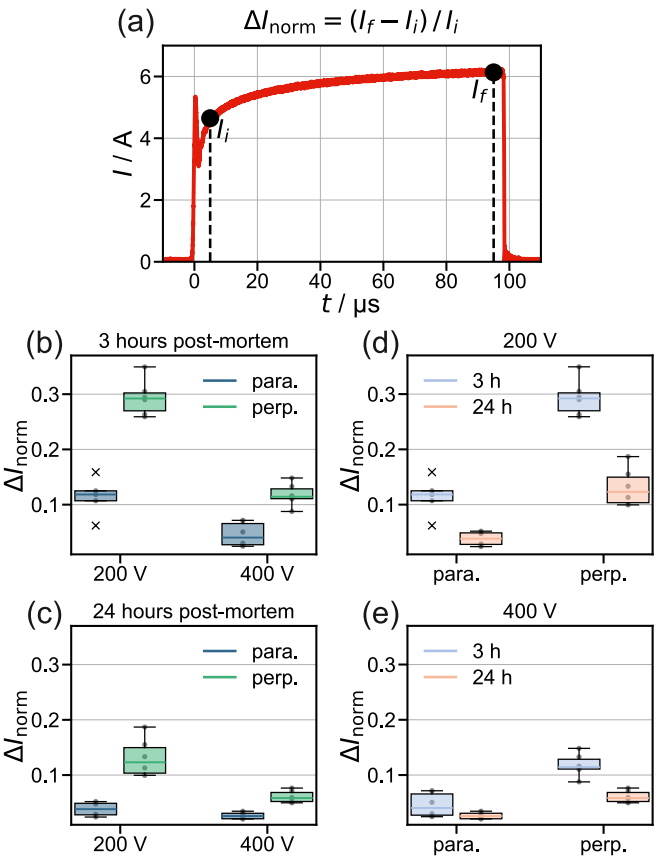

Fig. 5. (a) The definition of the normalised electric current difference (ΔI_{norm}), calculated as the difference between the final (I_f; at t = 95 μs) and the initial (I_i; at t = 5 μs) current values of the first electroporation pulse delivered, divided by the initial current value (I_i). The calculated normalised electric current for the parallel (i.e., the impedance was measured in the direction parallel to the muscle fibres) and the perpendicular (i.e., the impedance was measured in the direction perpendicular to the muscle fibres) orientations at (b) 3 h post-mortem and (c) 24 h post-mortem. Electroporation was performed using 8 rectangular pulses, each with a duration of 100 μs, an amplitude of either 200 V or 400 V, and a pulse repetition rate of 1 s^{-1}. The results are presented as boxplots, with the median marked by the centre line, the box representing the interquartile range (IQR), and the whiskers extending to the most extreme values within 1.5 × IQR. Outliers, which are marked as individual points, are values beyond 1.5 × IQR. $N = 6$.

The differences observed between the orientations can be attributed to the role of the cell plasma membranes in determining the tissue's electrical response. In the perpendicular orientation, the membranes act as significant barriers to current flow, and their electroporation leads to greater conductivity changes. In contrast, in the parallel orientation, the current bypasses the membranes, resulting in smaller changes in conductivity.

The differences between the 3-h and 24-h post-mortem samples illustrate the influence of tissue degradation. At 3 h post-mortem, the better-preserved tissue structure and membrane integrity allow a more pronounced electroporation. In contrast, the degradation of cellular and extracellular components 24 h post-mortem impairs membrane function, resulting in a lower ability of the tissue to undergo electroporation and a smaller change in current dynamics.

These results emphasise the critical role of tissue orientation and integrity in determining the electrical response during electroporation. The perpendicular orientation showed more pronounced changes in conductivity, and the effects were more pronounced at earlier stages and became less significant as the tissue degraded.

3.4. Numerical modelling results and comparison with experimental measurements

Fig. 6 compares the modelling results with the experimentally determined frequency-dependent impedance of the untreated skeletal muscle in both the parallel and perpendicular orientations. The modelling results for 3 h and 24 h post-mortem are shown in Fig. 6b and d, respectively, while the experimental data are shown in Fig. 6a and c, respectively.

The best fit of the experimental data in the perpendicular orientation was obtained using the least mean squares method, which yielded a membrane conductivity of $\sigma_m = 5 \times 10^{-7}$ S/m for the 3 h post-mortem samples (Fig. 6b). The other curves, shown in lighter hues, correspond to different membrane conductivity values ranging from 1×10^{-8} S/m to 1×10^{-6} S/m, illustrating how the impedance changes with variations in membrane conductivity.

For the 24-h post-mortem data (Fig. 6d), the best fit to the experimental results was achieved with a membrane conductivity of $\sigma_m = 1 \times 10^{-4}$ S/m. The other curves correspond to membrane conductivity values between 0.6×10^{-4} S/m and 1.4×10^{-4} S/m. The effect of the membrane conductivity on the parallel orientation is negligible at both time points.

In general, the modelling results are in agreement with the experimental data, suggesting that the numerical model accurately reflects the general trends of the frequency-dependent impedance of the untreated skeletal muscle. However, a slight difference is observed between the experimental and modelling results, particularly in the parallel orientation and at higher frequencies in the perpendicular orientation, where the impedance values are higher in the modelling results. This discrepancy suggests that the intra- and extracellular conductivities of the tissue sample in our experiments were likely higher than the values used in the model, which could explain the observed differences at these frequencies.

The experimental curves (Fig. 6a and c) decrease more gradually with frequency than the simulated curves (Fig. 6b and d). This is consistent with the intrinsic heterogeneity of skeletal muscle: variations in fibre size, the presence of non-myocyte cells and capillaries, and layered connective tissue all contribute to a broader dispersion of characteristic frequencies. In addition, post-mortem time-dependent changes in membrane integrity further broaden the measured response. A small dispersion of fibre orientations within the sample leads to averaging over slightly different angles, making the measured response broader and smoother. In our simulations, we intentionally assume a single, uniform fibre population with fixed intra- and extracellular properties and frequency-independent membrane parameters; this simplification narrows the response and leads to a steeper transition. Some additional smoothing in the measurements probably results from averaging over the samples (with $N = 12$).

The numerical modelling results obtained provide a useful framework for understanding the experimental impedance data, particularly the changes observed over time as the tissue degrades. The sensitivity of the model to membrane conductivity is consistent with the experimental observations of post-mortem tissue degradation [55] and supports the idea that membrane integrity plays a critical role in determining the

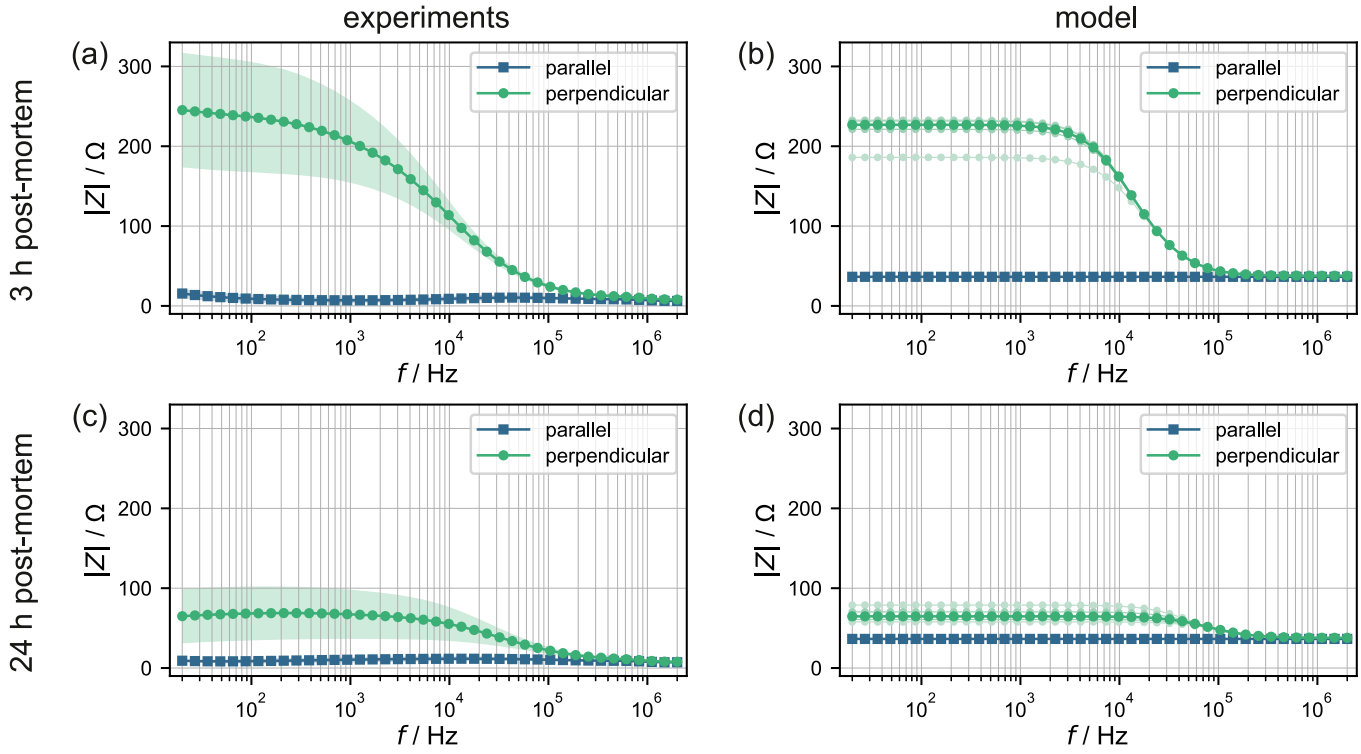

Fig. 6. Frequency-dependent absolute impedance of untreated skeletal muscle in the parallel (i.e., the impedance was measured in the direction parallel to the muscle fibres) and the perpendicular (i.e., the impedance was measured in the direction perpendicular to the muscle fibres) orientations. The experimentally determined impedance is shown in (a, c), while the corresponding modelling results are shown in (b, d). The results for 3 h post-mortem are shown in (a, b), and for 24 h post-mortem in (c, d). The experimental results are given as mean values ± standard deviations (shaded areas), with N = 12. In (b), the best fit of the perpendicular orientation to the corresponding experimental data (shown in green) corresponds to a membrane conductivity of $\sigma_m = 5 \times 10^{-7}$ S/m. The other curves (shown in lighter hue) correspond to membrane conductivity values, from the highest to the lowest impedance, of 1×10^{-8} S/m, 1×10^{-7} S/m, 1×10^{-6} S/m, and 5×10^{-6} S/m, respectively. In (d), the best fit of the perpendicular orientation to the corresponding experimental data (shown in green) corresponds to a membrane conductivity of $\sigma_m = 1 \times 10^{-4}$ S/m. The other curves (shown in lighter hue) correspond to membrane conductivity values, from the highest to the lowest impedance, of 0.6×10^{-4} S/m, 0.8×10^{-4} S/m, 1.2×10^{-4} S/m, and 1.4×10^{-4} S/m, respectively. The influence of the membrane conductivity on the parallel results is negligible. (For interpretation of the references to colour in this figure legend, the reader is referred to the Web version of this article.)

electrical properties of skeletal muscle.

It is also important to consider the uncertainty in the conductivity and permittivity values of the individual tissue constituents, i.e., intracellular space, extracellular space, and membranes, used in the model. The data for these tissue constituents are not precisely known and may vary due to tissue heterogeneity and post-mortem changes. The values used in the model are based on literature, which may not fully capture the variations due to tissue heterogeneity and post-mortem changes. Additionally, the values in literature also vary considerably. This uncertainty in the material properties could contribute to the observed discrepancies between the experimental and modelling results, which seem especially evident at higher frequencies where the calculated impedance is higher than the experimental one, suggesting that the values of intra- and extracellular conductivities used in the model are too low. Nevertheless, the model provides a useful framework for understanding the overall trends in the impedance data, with sensitivity to membrane conductivity being consistent with the experimental observations of post-mortem tissue degradation.

The reader should note that possible routes towards generalising the model and the experimental approach must consider that muscle tissues of different animal species, in general, degrade at different rates. These rates have been approximately determined for animals of interest as sources of meat and span a vast range; the fastest rates of decay (fish, chicken) can be up to an order of magnitude apart from the slowest (beef, lamb, deer) [77]. Our study did also not consider techniques of tissue conservation or preservation that have been developed mainly for the purposes of prolonging the viability of organs in organ donor programmes. Using some of those approaches, it should be feasible to considerably extend the window of usefulness of excised tissue samples from just a couple of hours to possibly several days [78].

Beyond ex vivo characterisation, impedance spectroscopy combined with our numerical model also offers a significant potential for the characterisation of in vitro engineered muscle tissues, an area expected to drive breakthroughs in regenerative medicine, wound healing, and biohybrid robots [79–82]. At present, assessment of these in vitro tissues relies mainly on contraction-force measurements or morphological analysis; although valuable, these methods can be destructive or provide limited insight into cellular maturation. Integrating impedance spectroscopy would provide a complementary, non-destructive method, while the numerical model helps to interpret the complex impedance data and relate it to cellular-level properties such as membrane integrity, effective cell density, and fibre alignment, which are key indicators of tissue functionality.

3.5. Numerical modelling predictions for intermediate fibre orientations

To demonstrate the predictive ability of the model for complex, multi-angular muscle architectures (e.g., multipennate muscles), we simulated the frequency-dependent impedance at 0°, 15°, 30°, 45°, 60°, 75°, and 90° relative to the fibres for two post-mortem times (3 h, with $\sigma_m = 5 \times 10^{-7}$ S/m; and 24 h, with $\sigma_m = 1 \times 10^{-4}$ S/m) (Fig. 7). At both time points, the absolute impedance increases uniformly with the angle from the parallel (0°) to the perpendicular (90°) orientation, with the largest differences between the angles occurring at low to medium frequencies. At 3 h post-mortem, the lower conductivity of the membranes emphasises the resistance at low frequencies and results in a more pronounced transition between angles; at 24 h post-mortem, the higher conductivity of the membranes flattens the response and slightly compresses the angular spread. The parallel orientation remains comparatively insensitive to membrane conductivity, whereas the perpendicular and intermediate orientations show a more pronounced dependence. These results illustrate how the model can predict responses for complex multi-angle architectures, and highlight its utility when experimental characterisation is challenging.

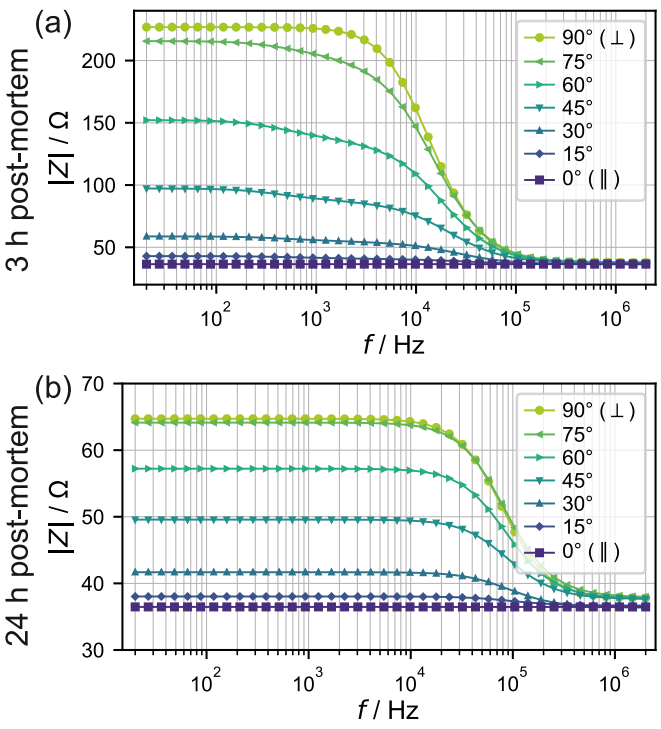

Fig. 7. The modelling results of frequency-dependent absolute impedance of untreated skeletal muscle in the parallel (i.e., the impedance was measured in the direction parallel to the muscle fibres; 0°), the perpendicular (i.e., the impedance was measured in the direction perpendicular to the muscle fibres; 90°), and intermediate orientations in 15° steps (15°, 30°, 45°, 60°, 75°). The results are shown for two post-mortem times: (a) 3 h with membrane conductivity fixed at $\sigma_m = 5 \times 10^{-7}$ S/m; and (b) 24 h with $\sigma_m = 1 \times 10^{-4}$ S/m. Note the different ordinate scales at (a) 3 h and (b) 24 h post-mortem.

4. Conclusions

We primarily set up our study to assess if it is possible to investigate anisotropy in skeletal muscle tissue ex vivo using impedance spectroscopy on an excised muscle, post-mortem. If an animal is slaughtered in the process of meat production for human consumption, the experiment does not require sacrificing an animal expressly for scientific purposes. Our study suggests that perhaps some of the live animal experiments, where and if deemed suitable, could be replaced by ex vivo work, thereby reducing moral and economic cost of animal experimentation. The approach certainly beats potato models that are currently used when animal experimentation is not feasible or justifiable [83].

Secondly, we built a model to validate the experimental results where we constructed a structured bundle of muscle fibres in silico and showed that anisotropy in electrical impedance is a direct result of skeletal muscle geometry if we account for typical intra- and extracellular conductivities of muscle cells and – most importantly – the low conductivity of the living cell plasma membrane.

And thirdly, we have shown through comparison of muscle anisotropy changes resulting from tissue dying and thus undergoing degradation processes versus those resulting from increasing cell membrane permeability by electroporation that these processes both affect the membrane permeability in a similar way, resulting in a like decrease in muscle anisotropy. We have thus shown that a single variable – i.e. the (im)permeability of the muscle cell membrane for ions – is responsible for the observed bulk tissue anisotropy in electrical impedance of skeletal muscle.

Possible limitations of the model and the experimental study mainly stem from its lack of comprehensiveness. The study should be understood as a proof of concept. Much work remains in characterising the

dynamics of skeletal muscle electric impedance anisotropy changes for different muscle origins (species of animal, type of muscle, …) and handling of the tissue after excision (temperature, preservation solution, …). We relegate these endeavours to future work.

CRediT authorship contribution statement

Rok Šmerc: Writing – review & editing, Writing – original draft, Visualization, Validation, Software, Resources, Methodology, Investigation, Formal analysis, Conceptualization. **Damijan Miklavčič:** Writing – review & editing, Supervision, Funding acquisition. **Samo Mahnič-Kalamiza:** Writing – review & editing, Writing – original draft, Supervision, Resources, Methodology, Investigation, Conceptualization.

Ethics statement

Samples of skeletal muscle tissue used in the ex vivo part of the study were obtained from a local slaughterhouse. The obtained samples were intended exclusively as animal food products and are therefore regulated by the Animal Protection Act (Official Gazette of the Republic of Slovenia, No. 38/13), which ensures ethical standards for animal slaughter, and are in accordance with Council Regulation (EC) No. 1099/2009 on the protection of animals at the time of killing. Consequently, there are no ethical concerns regarding the use of such samples in the experiments.

Declaration of competing interest

Damijan Miklavčič is the inventor and author of several patents pending and granted, is receiving royalties, and is consulting for several companies and organizations, which are active in electroporation and electroporation-based technologies and therapies. Other authors report no conflict of interest.

Acknowledgements

This work was supported by Slovenian Research and Innovation Agency (ARIS) through University of Ljubljana's internal funding for Start-up Research Programmes and grant P2-0249 Electroporation-based technologies and treatments. This study was conducted within the Infrastructure Programme: Network of research infrastructure centres at the University of Ljubljana (MRIC UL IP-0510), specifically within infrastructural centre Cellular Electrical Engineering (I0-0022), also funded by the Slovenian Research and Innovation Agency (ARIS).

References

[1] S. Grimnes, Bioimpedance and Bioelectricity Basics, third ed., Academic Press, London, U.K, 2015.
[2] K.R. Foster, H.P. Schwan, Dielectric properties of tissues and biological materials: a critical review, Crit. Rev. Biomed. Eng. 17 (1989) 25–104.
[3] C. Gabriel, S. Gabriel, E. Corthout, The dielectric properties of biological tissues: I. Literature survey, Phys. Med. Biol. 41 (1996) 2231–2249, https://doi.org/10.1088/0031-9155/41/11/001.
[4] S. Gabriel, R.W. Lau, C. Gabriel, The dielectric properties of biological tissues: II. Measurements in the frequency range 10 Hz to 20 GHz, Phys. Med. Biol. 41 (1996) 2251–2269, https://doi.org/10.1088/0031-9155/41/11/002.
[5] S. Gabriel, R.W. Lau, C. Gabriel, The dielectric properties of biological tissues: III. Parametric models for the dielectric spectrum of tissues, Phys. Med. Biol. 41 (1996) 2271–2293, https://doi.org/10.1088/0031-9155/41/11/003.
[6] D. Miklavčič, N. Pavšelj, F.X. Hart, Electric properties of tissues, in: M. Akay (Ed.), Wiley Encyclopedia of Biomedical Engineering, first ed., Wiley, 2006 https://doi.org/10.1002/9780471740360.ebs0403.
[7] D.A. Dean, T. Ramanathan, D. Machado, R. Sundararajan, Electrical impedance spectroscopy study of biological tissues, J. Electrost. 66 (2008) 165–177, https://doi.org/10.1016/j.elstat.2007.11.005.
[8] M.B. Lee, G.-H. Jahng, H.J. Kim, E.J. Woo, O.I. Kwon, Extracellular electrical conductivity property imaging by decomposition of high-frequency conductivity at larmor-frequency using multi-b-value diffusion-weighted imaging, PLoS One 15 (2020) e0230903, https://doi.org/10.1371/journal.pone.0230903.
[9] H.S. Mayberg, A.M. Lozano, V. Voon, H.E. McNeely, D. Seminowicz, C. Hamani, J. M. Schwalb, S.H. Kennedy, Deep brain stimulation for treatment-resistant depression, Neuron 45 (2005) 651–660, https://doi.org/10.1016/j.neuron.2005.02.014.
[10] R. Banan Sadeghian, M. Ebrahimi, S. Salehi, Electrical stimulation of microengineered skeletal muscle tissue: effect of stimulus parameters on myotube contractility and maturation, J. Tissue Eng. Regen. Med. 12 (2018) 912–922, https://doi.org/10.1002/term.2502.
[11] D. Serrano-Muñoz, H. Beltran-Alacreu, D. Martín-Caro Álvarez, J.J. Fernández-Pérez, J. Aceituno-Gómez, R. Arroyo-Fernández, J. Avendaño-Coy, Effectiveness of different electrical stimulation modalities for pain and masticatory function in temporomandibular disorders: a systematic review and meta-analysis, J. Pain 24 (2023) 946–956, https://doi.org/10.1016/j.jpain.2023.01.016.
[12] R.M. Dorrian, C.F. Berryman, A. Lauto, A.V. Leonard, Electrical stimulation for the treatment of spinal cord injuries: a review of the cellular and molecular mechanisms that drive functional improvements, Front. Cell. Neurosci. 17 (2023) 1095259, https://doi.org/10.3389/fncel.2023.1095259.
[13] Y. Chen, C.-P. Liang, Y. Liu, A.H. Fischer, A.V. Parwani, L. Pantanowitz, Review of advanced imaging techniques, J. Pathol. Inf. 3 (2012) 22, https://doi.org/10.4103/2153-3539.96751.
[14] S. Hussain, I. Mubeen, N. Ullah, S.S.U.D. Shah, B.A. Khan, M. Zahoor, R. Ullah, F. A. Khan, M.A. Sultan, Modern diagnostic imaging technique applications and risk factors in the medical field: a review, BioMed Res. Int. 2022 (2022) 5164970, https://doi.org/10.1155/2022/5164970.
[15] R.V. Davalos, L.M. Mir, B. Rubinsky, Tissue ablation with irreversible electroporation, Ann. Biomed. Eng. 33 (2005) 223–231, https://doi.org/10.1007/s10439-005-8981-8.
[16] M.L. Yarmush, A. Golberg, G. Serša, T. Kotnik, D. Miklavčič, Electroporation-based technologies for medicine: principles, applications, and challenges, Annu. Rev. Biomed. Eng. 16 (2014) 295–320, https://doi.org/10.1146/annurev-bioeng-071813-104622.
[17] B. Geboers, H.J. Scheffer, P.M. Graybill, A.H. Ruarus, S. Nieuwenhuizen, R.S. Puijk, P.M. Van Den Tol, R.V. Davalos, B. Rubinsky, T.D. De Gruijl, D. Miklavčič, M. R. Meijerink, High-voltage electrical pulses in oncology: irreversible electroporation, electrochemotherapy, gene electrotransfer, electrofusion, and electroimmunotherapy, Radiology 295 (2020) 254–272, https://doi.org/10.1148/radiol.2020192190.
[18] T. Kotnik, G. Pucihar, D. Miklavčič, The cell in the electric field, in: S.T. Kee, J. Gehl, E.W. Lee (Eds.), Clinical Aspects of Electroporation, Springer New York, New York, NY, 2011, pp. 19–29, https://doi.org/10.1007/978-1-4419-8363-3_3.
[19] T. Kotnik, L. Rems, M. Tarek, D. Miklavčič, Membrane electroporation and electropermeabilization: mechanisms and models, Annu. Rev. Biophys. 48 (2019) 63–91, https://doi.org/10.1146/annurev-biophys-052118-115451.
[20] T. Batista Napotnik, T. Polajžer, D. Miklavčič, Cell death due to electroporation – a review, Bioelectrochemistry 141 (2021) 107871, https://doi.org/10.1016/j.bioelechem.2021.107871.
[21] S. Haberl, D. Miklavcic, G. Sersa, W. Frey, B. Rubinsky, Cell membrane electroporation-part 2: the applications, IEEE Electr. Insul. Mag. 29 (2013) 29–37, https://doi.org/10.1109/MEI.2013.6410537.
[22] S. Sachdev, T. Potočnik, L. Rems, D. Miklavčič, Revisiting the role of pulsed electric fields in overcoming the barriers to in vivo gene electrotransfer, Bioelectrochemistry 144 (2022) 107994, https://doi.org/10.1016/j.bioelechem.2021.107994.
[23] T. Kotnik, W. Frey, M. Sack, S. Haberl Meglič, M. Peterka, D. Miklavčič, Electroporation-based applications in biotechnology, Trends Biotechnol. 33 (2015) 480–488, https://doi.org/10.1016/j.tibtech.2015.06.002.
[24] S. Mahnič-Kalamiza, E. Vorobiev, D. Miklavčič, Electroporation in food processing and biorefinery, J Membrane Biol 247 (2014) 1279–1304, https://doi.org/10.1007/s00232-014-9737-x.
[25] G. Saldaña, I. Álvarez, S. Condón, J. Raso, Microbiological aspects related to the feasibility of PEF technology for food pasteurization, Crit. Rev. Food Sci. Nutr. 54 (2014) 1415–1426, https://doi.org/10.1080/10408398.2011.638995.
[26] L.M. Mir, M.F. Bureau, J. Gehl, R. Rangara, D. Rouy, J.-M. Caillaud, P. Delaere, D. Branellec, B. Schwartz, D. Scherman, High-efficiency gene transfer into skeletal muscle mediated by electric pulses, Proc. Natl. Acad. Sci. USA 96 (1999) 4262–4267, https://doi.org/10.1073/pnas.96.8.4262.
[27] G. Tevz, D. Pavlin, U. Kamensek, S. Kranjc, S. Mesojednik, A. Coer, G. Sersa, M. Cemazar, Gene electrotransfer into Murine skeletal muscle: a systematic analysis of parameters for long-term gene expression, Technol. Cancer Res. Treat. 7 (2008) 91–101, https://doi.org/10.1177/153303460800700201.
[28] D.C. Hughes, J.P. Hardee, D.S. Waddell, C.A. Goodman, CORP: gene delivery into murine skeletal muscle using in vivo electroporation, J. Appl. Physiol. 133 (2022) 41–59, https://doi.org/10.1152/japplphysiol.00088.2022.
[29] V.Y. Reddy, E.P. Gerstenfeld, A. Natale, W. Whang, F.A. Cuoco, C. Patel, S. E. Mountantonakis, D.N. Gibson, J.D. Harding, C.R. Ellis, K.A. Ellenbogen, D. B. DeLurgio, J. Osorio, A.B. Achyutha, C.W. Schneider, A.S. Mugglin, E. M. Albrecht, K.M. Stein, J.W. Lehmann, M. Mansour, Pulsed field or conventional thermal ablation for paroxysmal atrial fibrillation, N. Engl. J. Med. 389 (2023) 1660–1671, https://doi.org/10.1056/NEJMoa2307291.
[30] A. Verma, D.E. Haines, L.V. Boersma, N. Sood, A. Natale, F.E. Marchlinski, H. Calkins, P. Sanders, D.L. Packer, K.-H. Kuck, G. Hindricks, B. Onal, J. Cerkvenik, H. Tada, D.B. DeLurgio, On behalf of the PULSED AF investigators, pulsed field ablation for the treatment of atrial fibrillation: PULSED AF pivotal trial, Circulation 147 (2023) 1422–1432, https://doi.org/10.1161/CIRCULATIONAHA.123.063988.
[31] K.-R.J. Chun, D. Miklavčič, K. Vlachos, S. Bordignon, D. Scherr, P. Jais, B. Schmidt, State-of-the-art pulsed field ablation for cardiac arrhythmias: ongoing evolution and future perspective, Europace 26 (2024), https://doi.org/10.1093/europace/euae134 euae134.

[32] D. Miklavčič, A. Verma, P.R.P. Krahn, J. Štublar, B. Kos, T. Escartin, P. Lombergar, N. Coulombe, M. Terricabras, T. Jarm, M. Kranjc, J. Barry, L. Mattison, N. Kirchhof, D.C. Sigg, M. Stewart, G. Wright, Biophysics and electrophysiology of pulsed field ablation in normal and infarcted porcine cardiac ventricular tissue, Sci. Rep. 14 (2024) 32063, https://doi.org/10.1038/s41598-024-83683-y.
[33] Z.F. Bhat, J.D. Morton, S.L. Mason, A.E.-D.A. Bekhit, Current and future prospects for the use of pulsed electric field in the meat industry, Crit. Rev. Food Sci. Nutr. 59 (2019) 1660–1674, https://doi.org/10.1080/10408398.2018.1425825.
[34] L. Astráin-Redín, J. Raso, G. Cebrián, I. Álvarez, Potential of pulsed electric fields for the preparation of Spanish dry-cured sausages, Sci. Rep. 9 (2019) 16042, https://doi.org/10.1038/s41598-019-52464-3.
[35] R. Karki, I. Oey, P. Bremer, S.Y. Leong, P. Silcock, Effect of pulsed electric fields (PEF) pre-treatment on the quality of sous vide (SV) processed beef short ribs and optimisation of PEF and SV process parameters using multiple polynomial regression model, Food Bioprocess Technol. 16 (2023) 216–231, https://doi.org/10.1007/s11947-022-02932-y.
[36] I. Tomasevic, V. Heinz, I. Djekic, N. Terjung, Pulsed electric fields and meat processing: latest updates, Ital. J. Anim. Sci. (2023). https://www.tandfonline.com/doi/abs/10.1080/1828051X.2023.2206834. (Accessed 13 January 2025).
[37] B.R. Epstein, R.G. Settle, K.R. Foster, Anisotropic impedance properties of skeletal muscle, in: Bioengineering, Elsevier, 1981, pp. 139–143, https://doi.org/10.1016/B978-0-08-027207-8.50034-5.
[38] M.S. Spach, W.T. Miller, E. Miller-Jones, R.B. Warren, R.C. Barr, Extracellular potentials related to intracellular action potentials during impulse conduction in anisotropic canine cardiac muscle, Circ. Res. 45 (1979) 188–204, https://doi.org/10.1161/01.RES.45.2.188.
[39] D.B. Geselowitz, R.C. Barr, M.S. Spach, W.T. Miller, The impact of adjacent isotropic fluids on electrograms from anisotropic cardiac muscle. A modeling study, Circ. Res. 51 (1982) 602–613, https://doi.org/10.1161/01.RES.51.5.602.
[40] V. Tayfur, O. Magden, M. Edizer, A. Atabey, Anatomy of vastus lateralis muscle flap, J. Craniofac. Surg. 21 (2010) 1951–1953, https://doi.org/10.1097/SCS.0b013e3181f4ee7f.
[41] A. Rehfeld, M. Nylander, K. Karnov, Compendium of Histology: a Theoretical and Practical Guide, Springer International Publishing, Cham, 2017, https://doi.org/10.1007/978-3-319-41873-5.
[42] J. Malmivuo, R. Plonsey, Bioelectromagnetism Principles and Applications of Bioelectric and Biomagnetic Fields, Oxford University Press, 1995, https://doi.org/10.1093/acprof:oso/9780195058239.001.0001.
[43] M. Essone Mezeme, M. Kranjc, F. Bajd, I. Serša, C. Brosseau, D. Miklavčič, Assessing how electroporation affects the effective conductivity tensor of biological tissues, Appl. Phys. Lett. 101 (2012) 213702, https://doi.org/10.1063/1.4767450.
[44] Q. Castellví, B. Mercadal, A. Ivorra, Assessment of electroporation by electrical impedance methods, in: D. Miklavčič (Ed.), Handbook of Electroporation, Springer International Publishing, Cham, 2017, pp. 671–690, https://doi.org/10.1007/978-3-319-32886-7_164.
[45] A. Mercanzini, P. Colin, J.-C. Bensadoun, A. Bertsch, P. Renaud, *In Vivo* electrical impedance spectroscopy of tissue reaction to microelectrode arrays, IEEE Trans. Biomed. Eng. 56 (2009) 1909–1918, https://doi.org/10.1109/TBME.2009.2018457.
[46] H.S. Magar, R.Y.A. Hassan, A. Mulchandani, Electrochemical impedance spectroscopy (EIS): principles, construction, and biosensing applications, Sensors 21 (2021) 6578, https://doi.org/10.3390/s21196578.
[47] O. Kangasmaa, I. Laakso, Estimation method for the anisotropic electrical conductivity of in vivo human muscles and fat between 10 kHz and 1 MHz, Phys. Med. Biol. 67 (2022) 225002, https://doi.org/10.1088/1361-6560/ac9a1e.
[48] A. Ivorra, B. Rubinsky, In vivo electrical impedance measurements during and after electroporation of rat liver, Bioelectrochemistry 70 (2007) 287–295, https://doi.org/10.1016/j.bioelechem.2006.10.005.
[49] S. Laufer, A. Ivorra, V.E. Reuter, B. Rubinsky, S.B. Solomon, Electrical impedance characterization of normal and cancerous human hepatic tissue, Physiol. Meas. 31 (2010) 995–1009, https://doi.org/10.1088/0967-3334/31/7/009.
[50] A. Silve, A. Guimerà Brunet, B. Al-Sakere, A. Ivorra, L.M. Mir, Comparison of the effects of the repetition rate between microsecond and nanosecond pulses: electropermeabilization-induced electro-desensitization? Biochim. Biophys. Acta Gen. Subj. 1840 (2014) 2139–2151, https://doi.org/10.1016/j.bbagen.2014.02.011.
[51] T. García-Sánchez, A. Azan, I. Leray, J. Rosell-Ferrer, R. Bragós, LlM. Mir, Interpulse multifrequency electrical impedance measurements during electroporation of adherent differentiated myotubes, Bioelectrochemistry 105 (2015) 123–135, https://doi.org/10.1016/j.bioelechem.2015.05.018.
[52] T.A. Whitman, J.C. Forrest, M.T. Morgan, M.R. Okos, Electrical measurement for detecting early postmortem changes in porcine muscle, J. Anim. Sci. 74 (1996) 80, https://doi.org/10.2527/1996.74180x.
[53] C.E. Byrne, D.J. Troy, D.J. Buckley, Postmortem changes in muscle electrical properties of bovine M. longissimus dorsi and their relationship to meat quality attributes and pH fall, Meat Sci. 54 (2000) 23–34, https://doi.org/10.1016/S0309-1740(99)00055-8.
[54] X. Zhao, H. Zhuang, S.-C. Yoon, Y. Dong, W. Wang, W. Zhao, Electrical impedance spectroscopy for quality assessment of meat and fish: a review on basic principles, measurement methods, and recent advances, J. Food Qual. 2017 (2017) 1–16, https://doi.org/10.1155/2017/6370739.
[55] U. Pliquett, M. Altmann, F. Pliquett, L. Schöberlein, Py—A parameter for meat quality, Meat Sci. 65 (2003) 1429–1437, https://doi.org/10.1016/S0309-1740(03)00066-4.
[56] M. Pavlin, K. Flisar, M. Kandušer, The role of electrophoresis in gene electrotransfer, J Membrane Biol 236 (2010) 75–79, https://doi.org/10.1007/s00232-010-9276-z.
[57] Y. Lv, X. Cheng, S. Chen, H. Liu, Y. Wang, C. Yao, B. Rubinsky, Analysis of the electric field-dependent current during electroporation pulses, IEEE Access 8 (2020) 93850–93856, https://doi.org/10.1109/ACCESS.2020.2995151.
[58] D. Cukjati, D. Batiuskaite, F. André, D. Miklavčič, L.M. Mir, Real time electroporation control for accurate and safe in vivo non-viral gene therapy, Bioelectrochemistry 70 (2007) 501–507, https://doi.org/10.1016/j.bioelechem.2006.11.001.
[59] J. Langus, M. Kranjc, B. Kos, T. Šuštar, D. Miklavčič, Dynamic finite-element model for efficient modelling of electric currents in electroporated tissue, Sci. Rep. 6 (2016) 26409, https://doi.org/10.1038/srep26409.
[60] K.A. Poulsen, J.F. Young, P. Theil, M. Kolko, N. Oksbjerg, I.H. Lambert, Role of phospholipase A2 in the induction of drip loss in porcine muscle, J. Agric. Food Chem. 55 (2007) 1970–1976, https://doi.org/10.1021/jf062341n.
[61] J. Genovese, M. Kranjc, I. Serša, M. Petracci, P. Rocculi, D. Miklavčič, S. Mahnič-Kalamiza, PEF-treated plant and animal tissues: insights by approaching with different electroporation assessment methods, Innov. Food Sci. Emerg. Technol. 74 (2021) 102872, https://doi.org/10.1016/j.ifset.2021.102872.
[62] J. Pingel, H.M. Kjer, F. Biering-Sørensen, R. Feidenhans'l, T.B. Dyrby, 3D synchrotron imaging of muscle tissues at different atrophic stages in stroke and spinal cord injury: a proof-of-concept study, Sci. Rep. 12 (2022) 17289, https://doi.org/10.1038/s41598-022-21741-z.
[63] R. Šmerc, D.A. Ramirez, S. Mahnič-Kalamiza, J. Dermol-Černe, D.C. Sigg, L. M. Mattison, P.A. Iaizzo, D. Miklavčič, A multiscale computational model of skeletal muscle electroporation validated using *In Situ* porcine experiments, IEEE Trans. Biomed. Eng. 70 (2023) 1826–1837, https://doi.org/10.1109/TBME.2022.3229560.
[64] G. Pucihar, T. Kotnik, B. Valič, D. Miklavčič, Numerical determination of transmembrane voltage induced on irregularly shaped cells, Ann. Biomed. Eng. 34 (2006) 642–652, https://doi.org/10.1007/s10439-005-9076-2.
[65] J. Dermol-Černe, T. Batista Napotnik, M. Reberšek, D. Miklavčič, Short microsecond pulses achieve homogeneous electroporation of elongated biological cells irrespective of their orientation in electric field, Sci. Rep. 10 (2020), https://doi.org/10.1038/s41598-020-65830-3.
[66] T. Kotnik, D. Miklavčič, T. Slivnik, Time course of transmembrane voltage induced by time-varying electric fields—a method for theoretical analysis and its application, Bioelectrochem. Bioenerg. 45 (1998) 3–16, https://doi.org/10.1016/S0302-4598(97)00093-7.
[67] L. Rems, M. Ušaj, M. Kandušer, M. Reberšek, D. Miklavčič, G. Pucihar, Cell electrofusion using nanosecond electric pulses, Sci. Rep. 3 (2013) 3382, https://doi.org/10.1038/srep03382.
[68] M. Scuderi, J. Dermol-Černe, T. Batista Napotnik, S. Chaigne, O. Bernus, D. Benoist, D.C. Sigg, L. Rems, D. Miklavčič, Characterization of experimentally observed complex interplay between pulse duration, electrical field strength, and cell orientation on electroporation outcome using a time-dependent nonlinear numerical model, Biomolecules 13 (2023) 727, https://doi.org/10.3390/biom13050727.
[69] Tissue frequency chart » IT'IS foundation, (n.d.). https://itis.swiss/virtual-population/tissue-properties/database/tissue-frequency-chart/(accessed December 19, 2024).
[70] R. Šmerc, M. Stručić, M. Kranjc, I. Serša, D. Miklavčič, S. Mahnič-Kalamiza, Electrical pathways through the intricate network of skeletal muscle fibres: insights from MRI-validated numerical modelling, IEEE Trans. Biomed. Eng. (2025) 1–11, https://doi.org/10.1109/tbme.2025.3572353.
[71] H. Kwon, J.A. Nagy, R. Taylor, S.B. Rutkove, B. Sanchez, New electrical impedance methods for the *in situ* measurement of the complex permittivity of anisotropic biological tissues, Phys. Med. Biol. 62 (2017) 8616–8633, https://doi.org/10.1088/1361-6560/aa8c95.
[72] H. Kwon, M. Guasch, J.A. Nagy, S.B. Rutkove, B. Sanchez, New electrical impedance methods for the in situ measurement of the complex permittivity of anisotropic skeletal muscle using multipolar needles, Sci. Rep. 9 (2019), https://doi.org/10.1038/s41598-019-39277-0.
[73] B. Kos, L. Mattison, D. Ramirez, H. Cindrič, D.C. Sigg, P.A. Iaizzo, M.T. Stewart, D. Miklavčič, Determination of lethal electric field threshold for pulsed field ablation in ex vivo perfused porcine and human hearts, Front. Cardiovasc. Med. 10 (2023) 1160231, https://doi.org/10.3389/fcvm.2023.1160231.
[74] S. Čorović, L.M. Mir, D. Miklavčič, In vivo muscle electroporation threshold determination: realistic numerical models and in vivo experiments, J Membrane Biol 245 (2012) 509–520, https://doi.org/10.1007/s00232-012-9432-8.
[75] S. Corovic, I. Lackovic, P. Sustaric, T. Sustar, T. Rodic, D. Miklavcic, Modeling of electric field distribution in tissues during electroporation, Biomed. Eng. Online 12 (2013) 16, https://doi.org/10.1186/1475-925X-12-16.
[76] L. Zang, K. Gu, X. Ji, H. Zhang, S. Yan, X. Wu, Effect of anisotropic electrical conductivity induced by fiber orientation on ablation characteristics of pulsed field ablation in atrial fibrillation treatment: a computational study, JCDD 9 (2022) 319, https://doi.org/10.3390/jcdd9100319.
[77] M. Greaser, W. Guo, Postmortem muscle chemistry, 63–78, https://doi.org/10.1201/b11479-7, 2012.
[78] S. Freitas-Ribeiro, R.L. Reis, R.P. Pirraco, Long-term and short-term preservation strategies for tissue engineering and regenerative medicine products: state of the art and emerging trends, PNAS Nexus 1 (2022) pgac212, https://doi.org/10.1093/pnasnexus/pgac212.
[79] S.-J. Park, M. Gazzola, K.S. Park, S. Park, V. Di Santo, E.L. Blevins, J.U. Lind, P. H. Campbell, S. Dauth, A.K. Capulli, F.S. Pasqualini, S. Ahn, A. Cho, H. Yuan, B.

M. Maoz, R. Vijaykumar, J.-W. Choi, K. Deisseroth, G.V. Lauder, L. Mahadevan, K. K. Parker, Phototactic guidance of a tissue-engineered soft-robotic ray, Science 353 (2016) 158–162, https://doi.org/10.1126/science.aaf4292.

[80] R. Raman, C. Cvetkovic, R. Bashir, A modular approach to the design, fabrication, and characterization of muscle-powered biological machines, Nat. Protoc. 12 (2017) 519–533, https://doi.org/10.1038/nprot.2016.185.

[81] B. Jo, K. Motoi, Y. Morimoto, S. Takeuchi, Dynamic and static workout of in vitro skeletal muscle tissue through a weight training device, Adv Healthcare Materials 13 (2024) 2401844, https://doi.org/10.1002/adhm.202401844.

[82] R. Kinjo, Y. Morimoto, B. Jo, S. Takeuchi, Biohybrid bipedal robot powered by skeletal muscle tissue, Matter 7 (2024) 948–962, https://doi.org/10.1016/j.matt.2023.12.035.

[83] A. Narkar, A. Kaboudian, Y. Ardeshirpour, M. Casciola, T. Feaster, K. Blinova, In vitro assay development to study pulse field ablation outcome using Solanum Tuberosum, IJMS 25 (2024) 8967, https://doi.org/10.3390/ijms25168967.